Anomalous diffusion in external-force-affected deterministic systems

Jin Liu [1], Kehui Sun [1,*] and Huihai Wang [2]
[1]*School of Physics, Central South University, Changsha 410083, China*
[2]*School of Electronic Information, Central South University, Changsha 410083, China*

(Received 1 March 2024; accepted 20 June 2024; published 17 July 2024)

This study investigates the impact of external forces on the movement of particles, specifically focusing on a type of box piecewise linear map that generates normal diffusion akin to Brownian motion. Through numerical methods, the research delves into the effects of two distinct external forces: linear forces linked to the particle's current position and periodic sinusoidal forces related to time. The results uncover anomalous dynamical behavior characterized by nonlinear growth in the ensemble-averaged mean-squared displacement (EAMSD), aging, and ergodicity breaking. Notably, the diffusion pattern of particles under linear external forces resembles an Ehrenfest double urn model, with its asymptotic EAMSD coinciding with the Langevin equation under linear potential. Meanwhile, particle movement influenced by periodic sinusoidal forces corresponds to an inhomogeneous Markov chain, with its external force amplitude and diffusion coefficient function exhibiting a "multipeak" fractal structure. The study also provides insights into the formation of this structure through the turnstiles dynamics.

DOI: 10.1103/PhysRevE.110.014204

I. INTRODUCTION

Diffusion is a common phenomenon in nature, with Brownian motion [1] being a standard example of normal diffusion, where the EAMSD of particles is proportional to time, i.e., $\langle x^2\rangle \sim t^\alpha$ with $\alpha = 1$. However, scientists have observed an increasing number of anomalous diffusion phenomena characterized by an exponent $\alpha \neq 1$. Subdiffusion with $\alpha < 1$ is more common in crowded environments like phospholipid bilayers [2], cytoplasm of biological cells [3], etc. Superdiffusion with $\alpha > 1$ demonstrates in scenarios such as molecular transport within cells [4], turbulence [5], and more.

Experimental data demonstrating diffusion phenomena are often effectively modeled by advanced concepts in stochastic theory, including continuous time random walks (CTRW) [6–9], Lévy walks [1,7,10–12], Langevin equations [7,13,14], or fractional Brownian motion [15,16]. Among these, CTRW is one of the most effective models for describing particle diffusion processes and has been successfully applied in various fields such as carrier transport in amorphous semiconductors [17], electron transfer [8], dispersion in turbulent systems [18], and more.

The Langevin equation is a specialized model that describes complex dynamics by fully considering the force acting on particles in a hot bath. According to Newton's second law, an over-damped Langevin equation is described as

$$\dot{x}_t = \frac{1}{\gamma}\xi_t, \tag{1}$$

where ξ_t is Gaussian white noise with a mean of zero.

Compared with the CTRW model, it has significant advantages in characterizing the influence of external force fields. Meanwhile, the relationship between the Langevin equation and the CTRW model is very close. It is known that the Langevin equation equivalent to the subdiffusion CTRW model is [19]

$$\dot{x}_s = \sqrt{2\sigma}\xi_s, \quad \dot{t}_s = \eta_s, \tag{2}$$

where x_s is the original process on the internal time s, and η_s is a completely biased α-stable Lévy noise [20]. t_s is α-stable subordinator, and σ is the diffusion coefficient. The time change process $y_t := x(s_t)$ is an equivalent description of the continuous limit form of the subdiffusion CTRW model with power-law waiting time, where s_t represents the inverse process of α-stable subordinator, that is, the inverse α-stable subordinator [21]. After combining Eq. (2), it is expressed as a single Langevin equation in physical time t [22]:

$$\dot{y}_t = \sqrt{2\sigma}\bar{\xi}_t, \tag{3}$$

where $\bar{\xi}_t = \int_0^{+\infty} \xi_\tau \delta(t - t_\tau) d\tau$ is the composite noise [22].

Most of the existing research focus on the movement of free particles [23], assuming that particles are unaffected by external forces in their environment. However, in nature, it is rare to find truly free particles, as they are almost always subjected to some forms of external force field [13,22,24–37]. These force fields can be time-dependent, position-dependent, constant, periodic, and so on. The motion of particles in an external force field typically deviates from Brownian motion, as these forces can either stimulate or inhibit particle diffusion, resulting in anomalous diffusion behavior.

While the behavior of particles under external forces has been studied in stochastic systems, there is limited research on the diffusion properties of deterministic chaotic particles

*Contact author: kehui@csu.edu.cn

in external forces [38,39]. Furthermore, the explanation of anomalous diffusion mechanisms in deterministic dynamical systems is also limited [40–48]. In deterministic systems, the simplest theoretical tool for generating normal diffusion may be a one-dimensional chaotic map, which differs from the diffusion phenomenon caused by traditional random walks. A particle trajectory with initial conditions can be generated by a chaotic iterative map, leading to the diffusion phenomenon:

$$x_{t+1} = x_t + f(x_t) \equiv F(x_t). \tag{4}$$

Specifically, for Eq. (4), it exhibits the following symmetric properties [44]: (i) $f(x)$ has inversion symmetry, i.e., $f(x) = -f(-x)$. (ii) for $F(x)$, it should be a discrete translational symmetry of $F(x+1) = F(x) + 1$.

The function $F(x_t)$ represents a one-dimensional map that dictates the transformation of a particle from position x_t to x_{t+1}. The diffusion characteristics of this map are solely determined by the function within the box and the initial position x_0, which will be elaborated upon in Sec. II. Geisel and Thomae argued that this encompasses a wide range of maps (4) [44], such as $f(x_t) = (2x_t)^z$ with $0 \leqslant x_t \leqslant 1/2$, which Eli Barkai examined in the context of the subdiffusion aging problem [48]. Additionally, for $f(x_t) = \sin(2\pi x_t)$, under sufficiently large damping, the differential equations describing Josephson junctions, phase-locked loop, or driven pendula [49,50] can be simplified as this iterative map [51,52]. Fujisaka *et al.* demonstrated that the coarse-grained probability distribution of the box Tent map tends towards a Gaussian distribution asymptotically [53].

In the case of the piecewise linear chaotic map

$$x_{t+1} = M_a(x_t) = \begin{cases} ax_t, & 0 < x_t \leqslant 1/2, \\ ax_t + 1 - a, & 1/2 < x_t \leqslant 1, \end{cases} \quad a > 0, \tag{5}$$

with a uniform slope, and it lifted onto $\mathbb{R}$ by $M_a(x_t + 1) = M_a(x_t) + 1$, and its diffusion coefficient exhibits a unique fractal structure [54,55]. Sato *et al.* investigated the impact of random noise on the system (5), where particles are randomly combined by sampling between a localized and a chaotic state, leading to their dynamical behavior displaying long-term anomalous dynamics [56].

This study focuses on examining the influence of external forces on the dynamics of the box piecewise linear chaotic map (5). First, we examined the impact of position-dependent linear external forces on particle diffusion properties, revealing that the particle motion space is considered a finite container. By establishing the relationship between the escape region and external forces, we demonstrated that linear external forces transform the force-affected system into the Ehrenfest double urn model. Second, we explored the dynamical behavior under periodic sinusoidal forces, observing fluctuations in its EAMSD linked to external forces, while still adhering to normal diffusion behavior overall. Furthermore, the diffusion coefficient and the amplitude function of external force display a distinctive "multipeak" fractal structure. These discoveries enhance our comprehension of diffusion phenomena in complex deterministic systems and offer novel research prospects in related domains.

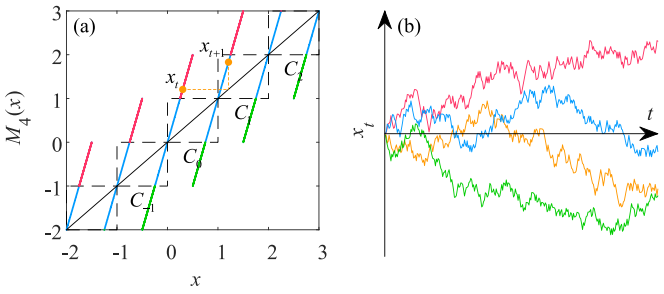

FIG. 1. Diffusion generated by a deterministic system (5) without external forces. (a) Particle trajectories exhibit chaotic oscillations within cells and chaotic diffusion between cells. The red and green line segments represent positive and negative escape regions, respectively. When a particle reaches the escape region, it will diffuse to the next neighboring cell at the next moment, as demonstrated by the yellow trajectory showing a single diffusion process of the particle. (b) The space-time plot displays four time series of particle trajectory positions at discrete time intervals $t \in \mathbb{N}$ under different initial conditions, resembling Brownian motion [56], with the parameter $a = 4$.

II. DETERMINISTIC DIFFUSION MODEL WITHOUT EXTERNAL FORCES

Although extensive discussions have been conducted on the properties of the map $M_a(x)$, for the coherence of this paper, it is necessary to provide a concise review and establish essential definitions to facilitate our subsequent discussion.

For $a > 2$, Eq. (5) exhibits normal diffusion, and its Lyapunov exponent is calculated as $\lambda(a) = \ln a$ [54,55]. Figure 1 illustrates the fundamental principle of chaotic particle diffusion in the systems, where an ensemble of solutions x_t diffusively motion resembling Brownian motion, with sample data obtained $x_{t+1} = M_4(x_t)$. In this scenario, $\lambda(4) = 4$. Through stretching and folding, Eq. (5) generates chaotic dynamical behavior on $\mathbb{R}$, and particle motion can be broken down into deterministic diffusion between boxes and chaotic oscillation within boxes. We use C_0, $C_{\pm1}$, $C_{\pm2}$, ... to encode these boxes distributed in the real number domain, as shown in Fig. 1(a). The length of these boxes is one, so they are also referred to as unit cells. The position of the particles is denoted as [53]

$$x_t = [x_t]_{\text{int}} + \tilde{x}_t, \tag{6}$$

where $[x_t]_{\text{int}}$ represents the largest integer smaller than x_t, and $\tilde{x}_t = x \mod 1$ possesses invariant density distribution within the cell, satisfying $0 \leqslant \tilde{x}_t \leqslant 1$ and $p(\tilde{x}) = 1$. Therefore, we can interpret $[x_t]_{\text{int}}$ as the position or momentum of particles, and $\tilde{x}_t$ as other degrees of freedom of particles or media.

The escape dynamics in chaotic systems demonstrate the correlation between the diffusion coefficient magnitude and the probability of particle escape from a box, specifically, the likelihood of jumping into another box [55]. This escape probability is exclusively linked to the parameters for Eq. (5). Sections III and IV will establish that the impact of an external force alters the particle escape probability within the cell, leading to the system's anomalous dynamical behavior.

For quantitative analysis, we partition the escape region within a cell into positive and negative escape regions. When

the particle is currently within this region and the next iteration is mapped to adjacent cells on the right, it is termed the positive escape region, with its corresponding interval labeled as the positive escape interval e_+. Conversely, the negative escape interval is denoted as e_-. Figure 1(a) illustrates the positive and negative escape regions using red and green line segments, respectively.

Within a cell, $M_4(x)$ exhibits positive and negative escape intervals with a length exactly equal to 1/4 of the cell length. It implies that the probability of particles escaping to adjacent cells at each iteration can be calculated as $p_e = 1/2$, and the escape probabilities in the positive and negative directions as $p_{e_+} = p_{e_-} = 1/4$. According to the central limit theorem, over a sufficiently long timescale, the diffusion distance conforms to a Gaussian distribution, and the diffusion type is a normal diffusion with $\alpha = 1$. The diffusion coefficient can be determined as $D = 0.25$ using $D = (1/24)(a-1)(a-2)$ [54,55].

In Fig. 1(b), the solutions of Eq. (5) at various initial positions demonstrate a deterministic diffusion motion, similar to Brownian motion at the macroscopic scale. Chaotic systems exhibit complete irregularity in their trajectories due to extreme sensitivity to initial conditions, yet their large sample data still demonstrate certain statistical characteristics.

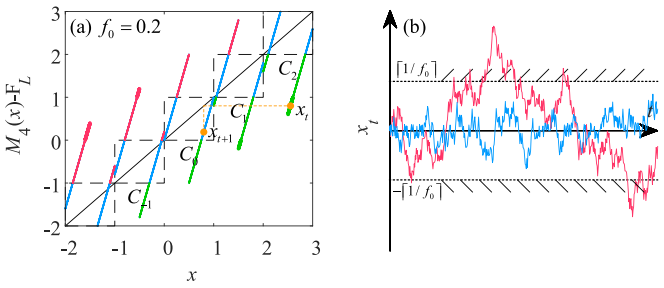

FIG. 2. (a) When $f_0 = 0.2$, the variation in particle motion space is different from the uniform medium shown in Fig. 1(a). Apart from cell C_0, the escape regions in each cell are biased. In the positive direction of cell C_0, the negative escape region expands, the positive direction interval shortens, and a new negative escape region with a jump amplitude of two cells is generated, and vice versa. (b) The solution displays the motion of two particles starting from the same position under different external force intensities, where the blue trajectory represents the particle experiencing a greater f_0, and the dashed line represents its constrained motion space. This suggests that the particle diffusion is akin to a random walk with a reflective wall. When a particle reaches the boundary, its next step can only remain in place or be reflected.

III. ANOMALOUS DYNAMIC IN LINEAR FORCE

In the natural motion of particles, the idealized motion scene depicted in Fig. 1 is highly simplified, and particle motion is inevitably influenced by external forces. It is widely recognized that many works often treat external forces as constants. However, research indicates that external forces may be associated with various factors, with one common type being position-dependent external forces [57,58]. This section explores the potential for deterministic anomalous dynamics in a system under a linear external force that is dependent on the particle's position.

We examine a system subjected to a linear external force $F_L = f_0([x_t]_{\text{int}})$, which is contingent on the current position of the particle in the cells, and continuously impacts the motion process. The model of the force-affected system is defined as

$$x_{t+1} = M_4(x_t) - F_L, \tag{7}$$

where F_L generates an external force akin to friction, and f_0 represents the intensity of the linear external force.

For the force-affected system (7), a subtle change has occurred in the particle diffusion model as sketched in Fig. 2(a). When a particle is subjected to a linear external force F_L directed towards cell C_0, the probability of its diffusion towards C_0 is greater when it moves away from C_0, due to the change in its escape region. In cell C_i, $i \in \mathbb{N}^*$, its positive escape interval e_+ is shortened, while the negative escape interval e_- is lengthened, and a new negative escape interval with a jump amplitude of two cells is generated, denoted as e_{2-}, which corresponds to the thick solid line in Fig. 2(a). When the particle falls into this region, it will be iterated to the previous two cells at the next moment, as shown by the orange particle trajectory in the figure. Conversely, in cell C_{-i}, e_+ is lengthened, e_- is shortened, and a new positive escape interval e_{2+} appears.

The blue and red trajectories in Fig. 2(b) show the diffusion diagrams of particles under different external force intensities, with the same initial position. The blue trajectory corresponds to a higher external force intensity, where the dashed line represents the range of motion of the particles on the blue trajectory, which is a finite area. The relationship between the particle diffusion trajectory and the external force intensity is $x_t \in [\lceil 1/f_0 \rceil, -\lceil 1/f_0 \rceil]$, where $\lceil 1/f_0 \rceil$ represents the smallest integer greater than or equal to $1/f_0$. Meanwhile, when the external force intensity is smaller, its diffusion range is larger, as shown in the red trajectory. The range of motion is not shown in the figure, where the particle is similar to a motion in a finite container. A smaller external force intensity enables the particle to diffuse in a larger container.

The impact of external forces only results in changes in the escape region, while maintaining an equal distribution property within the cells [59], which ensures that $x_t \mod 1$ possesses an invariant density. To further analyze the dynamical behavior of system (7), it is essential to examine the correlation between its escape interval, the intensity of the external force f_0, and the particles' positions. For instance, when considering an external force intensity of $f_0 = 0.5$, the particle's range of motion is $N_t = [-2, 2]$, as illustrated in Fig. 3.

Due to the linear nature of the external force in relation to symmetry, any alterations in the escape intervals on both sides of C_0 exhibit spatial symmetry. Consequently, our focus lies on the transition probability at C_i, $i \in \mathbb{N}^*$, leading to $r_i = 0.5 - 0.25 f_0 i$, $p_{i,i+1} = 0.25 - 0.25 f_0 i$, $q_{i,i-1} = 0.25 + 0.25 f_0 i$, and $q_{i,i-2} = 0.25 f_0 i$.

This implies that the diffusion probability in different cells is directly proportional to the external forces and their spatial positions, i.e., $p_e \propto f_0 i$. Under a constrained external force (typically $f_0 \leqslant 1$, as otherwise, particles remain within C_0 and $C_{\pm 1}$), we specifically examine scenarios where the external force's intensity is positive. In such cases, the greater the

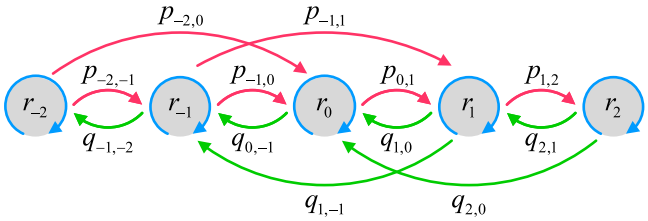

FIG. 3. The movement of particles due to external forces can be compared to a viscous Ehrenfest double urn model. When a particle is in cell C_i, there is a probability r_i that it will stay in place, a probability $p_{i,i+1}$ that it will diffuse to the adjacent positive cell (if the particle is not at the positive boundary), and a probability $q_{i,i-1}$ that it will diffuse to the neighboring negative cell (if the particle is not at the negative boundary). Additionally, the particle also has a probability $p_{i,i+2}$ or $q_{i,i-2}$ of moving to the two previous cells (depending on its current position).

relative displacement of particles, the stronger the compressive force they encounter, prompting them to gravitate towards C_0. Consequently, particles display a tendency to move towards the center, aligning with an equilibrium distribution. Intuitively, symmetry often coincides with conservation, as depicted by the particle motion trajectory in Fig. 2(b).

The process depicted in Fig. 3 can be considered a homogeneous Markov chain, effectively explained by the Ehrenfest double urn model [60,61]. The one-step transition probability matrix is represented as a $2\lceil 1/f_0 \rceil + 1$ order square matrix P, and the t-step transition matrix is computed using the Chapman-Kolmogorov equation [62–64] as

$$P^{(t)} = P^t, \tag{8}$$

where $P^{(t)}$ denotes the t-step transition matrix, and P^t denotes the t-power of the one-step transition matrix P.

For Eq. (8), we can utilize $P^t = U\Lambda^t V$ for calculation, where Λ is the diagonal matrix composed of the eigenvalues of P, square matrix $U \equiv [u_1, u_2, \cdots, u_N]$, and $V = U^{-1} \equiv [v_1, v_2, \cdots, v_N]^T$. As the sum of any row of P is 1, i.e., $\max|\Lambda| = 1$, then

$$\lim_{t\to\infty} \Lambda^t = \begin{bmatrix} 1 & 0 & \cdots & 0 \\ 0 & 0 & \cdots & 0 \\ \vdots & \vdots & \ddots & 0 \\ 0 & 0 & \cdots & 0 \end{bmatrix}, \tag{9}$$

the final $\lim_{t\to\infty} P^t = u_1 v_1$ will converge to the matrix with rank one.

Assuming the initial distribution is $p^{(0)}$, the probability distribution after t-step is $p^{(t)} = p^{(0)}P^{(t)}$, where $p^{(t)}$ represents the distribution of points on the line. Consequently, when $t \to \infty$, $p^{(t)}$ will ultimately converge to a stationary distribution independent of the initial distribution. It enables the calculation of the probability distribution when $f_0 = 0.01$, as depicted by the red curve in Fig. 4(a), consistent with the simulation results of the blue histogram graph $p(x)$ in the figure.

Figure 4(b) illustrates the EAMSD of system (7) with different f_0. The system demonstrates anomalous diffusion behavior with a continuously decaying diffusion exponent α.

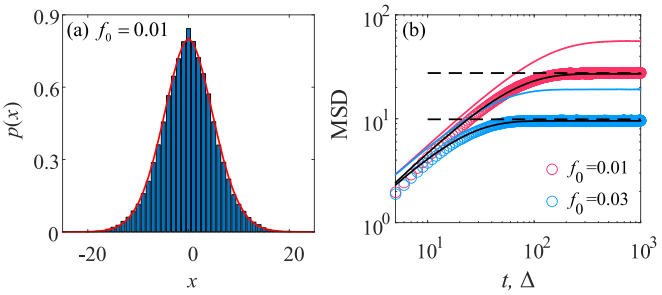

FIG. 4. The deterministic diffusion of system (7) is characterized by the probability distribution function (PDF) and mean-squared displacement (MSD). The MSD encompasses EAMSD, TAMSD, and the asymptotic MSD of the Langevin equation under external forces. Symbols are derived from trajectories of 10^7 uniformly distributed initial values x_0 on the C_0 unit cell over a duration of $t = 1000$. (a) The frequency distribution at $f_0 = 0.01$, depicted in the blue histogram, deviates from the Gaussian distribution. The red curve illustrates the theoretically calculated probability distribution, aligning with the frequency distribution. (b) EAMSD, under varying external force intensities, ultimately demonstrates a local diffusion of $\alpha = 0$. With larger external forces, EAMSD converges to smaller values more rapidly, consistent with the theoretically calculated EAMSD (black solid line). The black dashed line represents the theoretical asymptotic result of the Langevin equation under external force over an extended period of time [Eq. (18)]. The solid color lines represent TAMSD under the same parameters. The simulation parameters in Eq. (11) are set to $T = 3 \times 10^7$.

Over an extended period, due to the sustained action of external forces, the particles ultimately exhibit a local diffusion phenomenon with $\alpha = 0$, aligning with the earlier analysis of particle motion in a finite container. An increase in f_0 leads to a faster and smaller rate at which the system's EAMSD tends towards a steady-state value, corresponding to the localized diffusion process of particles in a smaller container, reflecting the expected dynamical behavior of particles. In discrete-time dynamical systems, EAMSD is defined as

$$\langle x_t^2 \rangle := \sum_{x=-\infty}^{+\infty} x^2 p(x,t). \tag{10}$$

By utilizing Eqs. (7) and (10), the theoretical asymptotic results for EAMSD are calculated, as depicted by the solid black line in Fig. 4(b), consistent with the simulation results represented by the colored circles. When f_0 is 0.01 and 0.03, it can be deduced from $\lim_{t\to\infty} p^{(t)} = p^{(t-1)}$ and Eq. (10) that EAMSD will converge to steady-state values, calculated as 27.0475 and 9.5376, respectively.

Moving on to another statistical measure, time-averaged mean-squared displacement (TAMSD), it was first determined by Nordlund in 1914 to ascertain the diffusion coefficient of tracer particles based on individual particle trajectories [65]. Since then, TAMSD has become a significant statistical indicator [7]. TAMSD is defined as

$$\overline{\delta_\Delta^2} = \frac{1}{T-\Delta} \sum_{t=0}^{T-\Delta} (x_{t+\Delta} - x_t)^2, \tag{11}$$

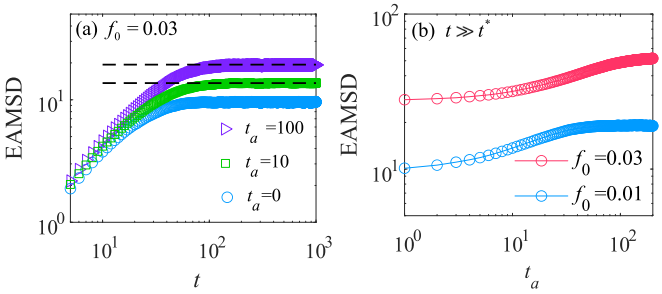

FIG. 5. The relationship between EAMSD and time varies at different observation times, (a) deviating from the standard CTRW model. The convergence value of EAMSD with t_a is closely linked to t_a and the critical time t^* with $t_a = 0$. The black dashed line depicts the theoretical asymptotic result of EAMSD over an extended period [see Eq. (14)]. (b) The convergence results of the particle's EAMSD at various observation times when $t \gg t^*$ and the EAMSD at $t_a \gg t^*$ are approximately twice that of $t_a = 0$, confirming the validity of Eq. (14). All other conditions remain unchanged as described in the caption of Fig. 4.

where Δ is the lag time, and T is the measurement time. To ensure favorable statistical characteristics, it is essential to satisfy $\Delta \ll T$. TAMSD reflects the long-term dynamical behavior of a single particle. When TAMSD equals EAMSD, it signifies that the long-term dynamical behavior of a single particle aligns with the general pattern of a large number of particles, indicating that the time statistical average of particles equals the spatial statistical average. We refer to particles as ergodic, otherwise, the motion process is considered to be ergodicity breaking [66,67].

The solid colored lines in Fig. 4(b) illustrate the TAMSD, with parameter values consistent with the colored circles. It is evident that TAMSD does not converge to EAMSD, indicating the breaking of ergodicity in the process. For certain stochastic processes in harmonic potentials, such as overdamped Brownian motion, fractional Brownian motion, and fractional-order Langevin equation, their TAMSD converges to twice the corresponding EAMSD after a prolonged period of evolution [68,69]. Intriguingly, deterministic force-affected system (7) also exhibit similar characteristics.

If the dynamical behavior of the system changes based on the initial observation time, it is considered to exhibit aging phenomenon [70,71]. In a dynamical process with aging phenomenon, the EAMSD is defined as

$$\left\langle x_t^2 \right\rangle_{t_a} = \left\langle \left(x_{t+t_a} - x_{t_a} \right)^2 \right\rangle, \tag{12}$$

where t_a represents the start time of observation.

Figure 5 illustrates the aging dynamics of particles at various observation times t_a. Specifically, Fig. 5(a) depicts the functional relationship between EAMSD and time t when $f_0 = 0.03$, while Fig. 5(b) demonstrates the gradual changes in EAMSD of the system over a long timescale at different observation times t_a. The findings indicate that EAMSD with $t_a > 0$ gradually converges to a constant value, approximately twice the convergence value of EAMSD with $t_a = 0$. According to the standard CTRW model for long times, $\langle x_t^2 \rangle \sim (t + t_a)^\alpha - t_a^\alpha$ [48], this theory further predicts that different observation times over an extended period will ultimately converge to a consistent EAMSD [44–48]. Hence, for system (7), it represents an aging phenomenon distinct from the standard CTRW model.

In reality, the EAMSD with $t_a > 0$ ultimately converges to $\langle x_t^2 \rangle_{t_a} = \langle x_t{}^2 \rangle + \langle x_{t_a}^2 \rangle$ over a long timescale. The black dashed line in Fig. 5(a) illustrates its asymptotic behavior, aligning with the simulation results. It is due to the fact that for systems with aging, their EAMSD is calculated as

$$\left\langle x_t^2 \right\rangle_{t_a} = \left\langle \left(x_{t+t_a} - x_{t_a} \right)^2 \right\rangle = \sum_{x=-\infty}^{+\infty} \left(x - x_{t_a} \right)^2 p(x, t), \tag{13}$$

and the above equation is expressed as

$$\left\langle x_t^2 \right\rangle_{t_a} = \left\langle x_t^2 \right\rangle + \left\langle x_{ta}^2 \right\rangle - 2x_{t_a} \sum_{x=-\infty}^{+\infty} x p\left(x - x_{t_a}, t \right). \tag{14}$$

Based on the analysis above, when $t \to \infty$, $p(x - x_{t_a}, t)$ eventually reaches a symmetrical stationary distribution independent of the initial distribution. Consequently, over an extended period, the last term of Eq. (14) can be considered as the first-order moment of variable x multiplied by $-2x_{t_a}$, resulting in a value of zero. Another intriguing observation is that when $t_a \gg t^*$, the EAMSD demonstrates nearly identical asymptotic values to TAMSD over extended timescales [Fig. 4(b)], where t^* denotes the critical time for the system to transition from subdiffusion to local diffusion, and at $f_0 = 0.03$, this critical time $t^* \approx 60$.

For systems with particle trajectories displaying ergodicity breaking properties, the CTRW model [6,9] may be a potential candidate for describing underlying physical mechanisms. However, the CTRW model primarily characterizes particle diffusion by defining the waiting time and the jump step PDF, thus lacking an intuitive description of particle motion under external force fields. Consequently, we employ the Langevin equation [19], equivalent to the subdiffusion CTRW model, to depict particle diffusion in a deterministic system under an external force. Reference [35] presents anomalous dynamical behavior in the Langevin equation under an external force field. As the primary reason for particles exhibiting subdiffusion is being trapped in the medium for a certain period, rendering them immobile, the particle's motion process can be perceived as a combination of waiting and jumping. Therefore, the ways in which external forces act on a subdiffusion stochastic process can be categorized into two types: intermittent external forces acting only when particles jump, and the other is that external forces continuously act on this subdiffusion process. The mathematical equations reflect the various ways external forces act in different physical realities: these external forces can be incorporated into the original process x_s in Eq. (2) or into the composite process y_t in Eq. (3).

In contrast to common intuition, it is necessary to consider the model in which external forces only come into play when particles undergo movement. When particles are confined and unable to move, external forces do not have an effect, which effectively accounts for this phenomenon. The corresponding Langevin equation is given by

$$\dot{x}_s = -\gamma x_s + \sqrt{2\sigma}\xi_s, \quad \dot{t}_s = \eta_s, \tag{15}$$

where γ is a positive constant, and the remaining variables are in line with Eq. (2). Here, the harmonic potential $U(x) = \gamma x^2/2$ leads to an external force $F(x) = -dU(x)/dx = -\gamma x$ akin to friction. As per Eq. (15), the single Langevin equation expression for the stochastic process $y_t := x(s_t)$ in the physical time t of the subordinated process is derived to

$$\dot{y}_t = -\gamma y_t \dot{s}_t + \sqrt{2\sigma}\bar{\xi}_t, \tag{16}$$

where $\bar{\xi}_t = \xi(s_t)\dot{s}_t$, and the EAMSD of y_t is expressed as [72]

$$\langle y_t^2 \rangle = \frac{\sigma}{\gamma} - \frac{\sigma}{\gamma} E_\alpha(-2\gamma t^\alpha), \tag{17}$$

where $E_\alpha(-2\gamma t^\alpha)$ represents the Mittag-Leffler function [73]. Through the utilization of the asymptotic expression of this function over an extended period, the asymptotic expression of EAMSD for the stochastic process y_t over a long period of time $t \gg (2\gamma)^{-1/\alpha}$ can be determined as

$$\langle y_t^2 \rangle \simeq \frac{\sigma}{\gamma} - \frac{\sigma}{2\gamma^2 \Gamma(1-\alpha)} t^{-\alpha}. \tag{18}$$

It implies that the EAMSD of the particle ultimately converges to the steady-state value $\langle y_t^2 \rangle = \sigma/\gamma$ over a power-law time.

Initially, by considering the diffusion exponent α and diffusion coefficient D of system (7) over a short timescale, for f_0 equal to 0.01 and 0.03, the diffusion exponent on a short timescale are 0.9240 and 0.8691, respectively. Subsequently, by using $D = 2\sigma/\Gamma(1+\alpha)$, we ascertain that σ is 0.2499 and 0.2419, respectively. By determining the convergence value $\langle y_t^2 \rangle = \sigma/\gamma$ of EAMSD over an extended period, the values of γ are 0.0090 and 0.0252, respectively. The asymptotic value of EAMSD for the Langevin equation under external forces can be derived as indicated by the dashed line in Fig. 4(b). It is consistent with the asymptotic value of EAMSD under the deterministic force-affected system represented by the colored circles, indicating that the diffusion characteristics of system (7) over long timescales are to some extent equivalent to a Langevin equation with a harmonic potential.

IV. ANOMALOUS DYNAMIC IN PERIODIC FORCE

Given that the system is exposed to a time-periodic sinusoidal force $F_S = A\sin(\Omega t)$ with amplitude A and angular frequency Ω, the deterministic equation of the system can be expressed as

$$x_{t+1} = M_4(x_t) - F_S. \tag{19}$$

The external force F_S in system (19) can be interpreted as a time-varying force, such as a frictional force that changes over time, with its period denoted as $2\pi/\Omega$.

It is important to note that fluctuations in friction have been extensively researched in various physical systems [74–76]. Friction is highly intricate, and extensive research [58,77–80] indicates that it is dependent on position, velocity, and temperature. Consequently, friction may vary based on these parameters. Some studies even demonstrate that specific frictional forces are influenced by the angular frequency of external forces [81], and certain frictional forces fluctuate over time [77]. It is evident that in many current studies, the friction coefficient is often assumed to be constant. However, certain research has indicated a strong correlation between specific friction coefficients and temperature [78,82], position [58], velocity, and external time-periodic forces, suggesting that in some systems, the friction coefficients are not constant but rather fluctuate over time [83–85].

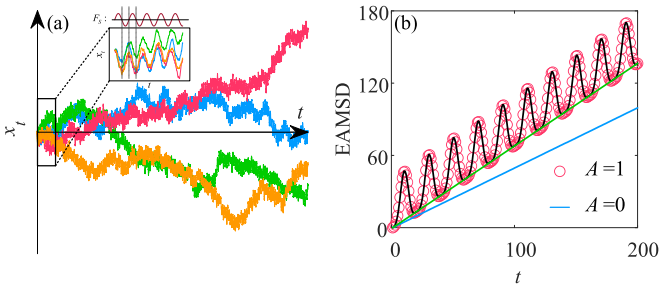

FIG. 6. The solution trajectory of system (19) and its EAMSD. (a) The trajectories of particle motion under external forces over a specific time period exhibit behavior similar to Brownian motion at a macroscopic scale. However, close examination reveals that particle fluctuations demonstrate a certain level of regularity within short time intervals, as indicated in the inset. (b) The red circle and blue line represent the EAMSD at $A = 1$ and 0, respectively. These symbols are derived from trajectories of 10^7 different initial values x_0 uniformly distributed on the C_0 unit cell over a duration of $t = 200$. The EAMSD demonstrates significant volatility under F_S, yet overall, it still adheres to a linear relationship. This linear relationship is depicted by the green line, and the diffusion coefficient function $D(A)$ in Fig. 8 is derived from this relationship.

To investigate how external forces, similar to friction, impact the dynamical behavior of a system, Fig. 6(a) depicts particle solutions under varying initial conditions, with amplitude $A = 1$ and frequency $\Omega = 0.1\pi$. The long-term behavior of the solutions resembles normal diffusion Brownian motion. However, the inset reveals a correlation between particle fluctuations and external forces, with the particle trajectory exhibiting periodic fluctuation, offset by half a phase from the change in external force F_S. It is due to the positive external force's influence when the external force F_S exceeds zero, causing particles to favor movement in the negative direction, and vice versa.

The inset in Fig. 6(a) reflects the contribution of external forces, resulting in periodic oscillations and additional displacement of particle positions. The trajectory resembles an antipersistent random walk [86,87], with a negative correlation of particle increments, indicating a higher probability of moving backward after a forward step. However, the behavior of system (19) is slightly different. The periodic polarity changes of the external forces result in delayed antipersistence. The increments of particles at time t and $t + 10$ exhibit negative correlation due to the half-phase difference of external forces directing the particles in two opposite directions. Denoting the particle increment as $\delta_t = x_t - x_{t-1}$, the two-dimensional probability density $p(\delta_t, \delta_{t+10})$ for δ_t and δ_{t+10} is depicted in Fig. 7(b), showing that a positive increment often leads to a negative increment after ten iterations, explaining the oscillatory motion trajectory of the particles. The one-dimensional increment PDF of the system, shown in the inset,

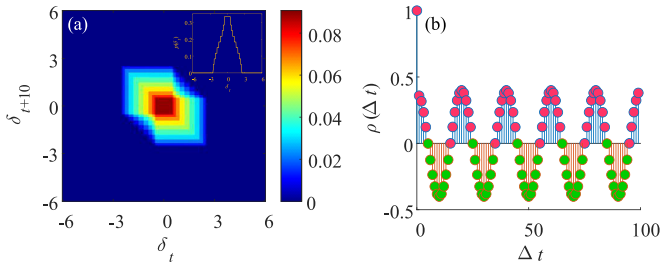

FIG. 7. (a) The two-dimensional probability density of $p(\delta_t, \delta_{t+10})$ for two increments δ_t and δ_{t+10} (main figure), and the one-dimensional probability density $p(\delta_t)$ are well described by a symmetric distribution with zero mean (inset). (b) The autocorrelation function $\rho(\Delta t)$ of the increments $\delta_t = x_t - x_{t-1}$ shows periodic peaks of alternating algebraic sign, clearly demonstrating delayed antipersistence.

indicates an average increment value of zero, resulting in pure diffusion without any drift. Additionally, Fig. 7(b) displays the autocorrelation function of the increments, demonstrating the predicted periodic changes aligned with the period of external forces. It confirms that a positive increment δ_t is more likely to result in a negative increment δ_{t+10} after ten iterations, clearly illustrating the system's delayed antipersistence.

In Fig. 6(b), the red circle represents the EAMSD with an external force amplitude $A = 1$. Unlike linear external forces [Fig. 4(b)], the EAMSD under periodic external forces shows periodic fluctuations, with an oscillation frequency consistent with F_S, while the blue line represents the EAMSD without external force. The overall growth trend of EAMSD under external forces still displays a linear relationship with time. We have fitted the local minimum value of EAMSD, indicated by the green line in the figure. Under external forces, the EAMSD fluctuates based on this green line, and it is evidently larger than the diffusion coefficient $D = 0.25$ (blue line) when not subjected to external forces.

As A increases from zero to six, the functional relationship $D(A)$ between external force amplitude A and diffusion coefficient D reveals a surprising and counterintuitive result, as shown by the purple curve in Fig. 8 [based on the EAMSD fitted by the green line in Fig. 6(b)]. In the long-term operation of the particles, the external force with zero mean neither balances $D(A)$ nor causes it to monotonically increased or decreased. Although the diffusion coefficient under the external force is significantly greater than that without external force,

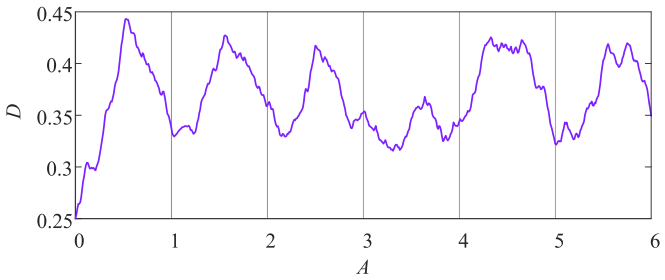

FIG. 8. The relationship between the diffusion coefficient D and the amplitude A of periodic external forces shows a continuous peak-like structure.

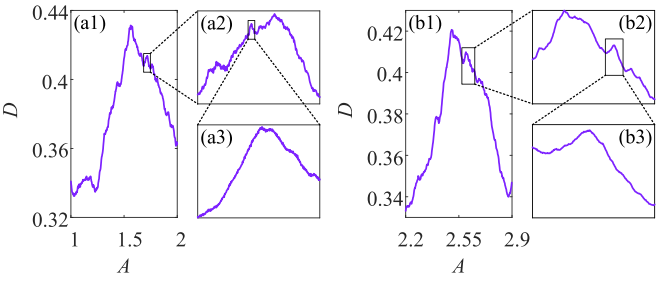

FIG. 9. The local amplification of the diffusion coefficient $D(A)$ related to the amplitude of external forces in system (19). (a1)–(a3) for $1 \leqslant A \leqslant 2$, and (b1)–(b3) for $2.2 \leqslant A \leqslant 2.9$. The structure still maintains a more intricate "mountain peak" pattern, demonstrating fractal characteristics at a specific scale.

its overall trend displays "multiple mountain" structures, with peaks and valleys generally located near half integers and integers, but there are also some exceptions. We observed that, in addition to integer and half-integer regions, local extrema also appear in certain areas, which piques our interest. Do these also represent local "peaks" or "valleys"?

Figure 9 displays the $D(A)$ curve within a more refined framework. It is evident that the variation in the diffusion coefficient remains quite pronounced at smaller scales, with local peaks and valleys recurrently emerging, indicating certain fractal characteristics. Before we explore the reasons for the emergence of this unique structure, it is essential to address a fundamental question: How many external factors truly influence the motion of the particle under the influence of a periodic sinusoidal force with an amplitude of A in the system? In other words, the long-term evolution of the system, due to external forces, makes it challenging to analyze the overall dynamical characteristics of the entire system as the particle's transmission medium varies over time. It is preferable to break down the dynamical characteristics of the system into simpler parts, analyze them from a microscopic perspective, and then characterize the overall dynamical characteristics of the entire system at a macro level.

The question at hand may seem obvious: for a system subjected to a periodic sinusoidal force, the magnitude and direction of the external force will repeat every period. Hence, the external force within one period can be considered as a sequence $F_S(A) = \{A\sin(0.1\pi t)|t = 0, 1, 2, \cdots, 19\}$. It is important to note that the elements in the $F_S(A)$ always appear in pairs as opposites.

Based on strong intuition, we believe that the characteristic $D(A)$ of system (19) can be comprehensively represented to some extent by the system (5) under the influence of the periodic pulse force. This is because if the sequence $F_S(A)$ is rearranged and a pair of opposite numbers is considered as the same external factor acting on the system (5), then the force-affected system (19) can be seen as continuously being acted upon by ten pairs of periodic pulse external force $F_P = A(-1)^t$ within one period. A deterministic system subjected to periodic pulse forces is described as

$$x_{t+1} = M_4(x_t) + A(-1)^t. \tag{20}$$

With this in mind, the details of the purple curve of $D(A)$ for the region $0 \leqslant A \leqslant 1$ are completed in Fig. 10, and the

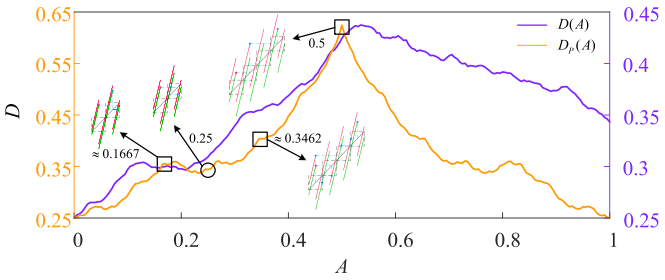

FIG. 10. The curves of $D(A)$ and $D_P(A)$ for $0 \leqslant A \leqslant 1$, including labels for significant parameter values that are related to "turnstile dynamics" (see text). Turnstile dynamics suggests, to some extent, a potential correlation between the local maxima and minima of $D(A)$ and $D_P(A)$, and the underlying microscopic chaotic scattering process. The main plot comprises data points with a step size of 0.005.

orange curve represents the diffusion coefficient $D_P(A)$ of the periodic pulse force-affected system (20).

Before delving into the structural characteristics of the $D(A)$, it is essential to comprehensively grasp the $D_P(A)$ curve. Clearly, the $D_P(A)$ curve exhibits symmetry around $A = 0.5$, suggesting a higher level of regularity compared to the $D(A)$ curve. Subsequently, a quantitative analysis of the $D_P(A)$ curve is conducted using the "turnstile dynamics" method [55].

Definition (turnstile). Turnstiles are the "coupling regions" of the single cells of a chain of class climbing box maps, where points of one unit interval get mapped outside that particular interval into another unit interval.

Through the examination of turnstile interactions and the manipulation of external force amplitudes, the research delves into whether particles can experience "favorable" or "unfavorable" escape conditions during their movement. Similar to Ref. [55], the extremum point $x = 1/2$ of the turnstile is utilized for analysis, and its mapping to the position of other turnstiles is calculated after a specific number of iterations.

To comprehend the impact of different external force amplitudes on particle diffusion motion, various typical external force amplitudes are selected, and the iterative data of particle trajectories under periodic pulse external force are presented in the insert of Fig. 10. These intensities are categorized into two types based on the analysis of the critical point $x = 1/2$ in system (20). Particles that contribute positively to escape are denoted by squares, while those with a negative impact on escape are represented by circles.

It is important to note that at $A \approx 0.1667$, a resemblance to the series γ mentioned in Ref. [55] is observed. The series γ is defined such that after one or several iterations, some points of $x = 1/2$ reach the right edge of the turnstile, i.e., $x = k + 1/2$, where k is an integer. In this scenario, the particle undergoes two iterations, reaching the right edge of the turnstile in the subsequent cell, located at $x = 3/2$. In the $D(a)$ curve (the function relationship between the diffusion coefficient and system parameters), the emergence of a series γ indicates the occurrence of a local maximum. Clearly, in the $D_P(A)$ curve, a series γ corresponds to a local maximum.

When $A \approx 0.3462$, the particle crosses three cells and reaches the right edge of the turnstile at $x = 7/2$, indicating that diffusion at this point also plays a promoting role. However, it does not strictly conform to the definition of series γ, so we classify it as a series γ-class. Similarly, at $A = 0.5$, it is also a series γ-class.

The figure illustrates multiple series γ and γ-class, but their impacts on particle escape velocity are not entirely equivalent. At $A \approx 0.1667$, the particle traverses one cell in two iterations, reaching $x = 3/2$. At $A \approx 0.3462$, the particle crosses three cells in six iterations, reaching $x = 7/2$. For $A = 0.5$, it only takes two iterations to reach $x = 7/2$. Evidently, they have different contributions to particle diffusion. It is important to note that for $0 \leqslant A \leqslant 1$, when a particle moves from one turnstile to another, the most efficient path is represented by the series γ or γ-class of $A = 0.5$. Therefore, the curve demonstrates a significant transition near $A = 0.5$, marking the appearance of the first main peak.

Reference [55] also introduces series α and β, which signify the particle reaching the leftmost turnstile in the next interval after one or more iterations. The emergence of these two series indicates a local minimum of $D(a)$. In reality, series α and β depict the particle starting at turnstile $x = 1/2$ and converging to a fixed point after a finite number of iterations, which negatively impacts the particle's escape. Similar dynamical characteristics are observed in the circles and their corresponding insets in Fig. 10. At $A = 0.25$, the particle converges to a period-2, signifying a slowdown of particle diffusion at this point, and correspondingly, the $D_P(A)$ curve displays a local minimum.

It is evident that the $D_P(A)$ curve can be divided into symmetric halves. In the $0 \leqslant A \leqslant 0.5$ range, the $D_P(A)$ curve generally increases with the rise of A, while on the right half of the curve, the opposite is true. Therefore, the extreme points analyzed earlier will also appear at the same positions on the right side of the curve, which will not be analyzed separately here.

The dynamical behavior of turnstiles in these specific areas provides a foundation for understanding the variation of $D_P(A)$ within the range of $0 \leqslant A \leqslant 1$ to a certain extent. However, another question arises: why does an external force (F_S or F_P) result in D values greater than 0.25, as indicated in system (19) and (20), when there is no external force? One possible explanation is that the $D(a)$ curve corresponds to a local minimum at $a = 4$, indicating a reduced efficiency for particle escape at this point. The external force from the surroundings then allows the particles to regain a higher escape efficiency. Therefore, even when the external force places the system in series α or β, the diffusion coefficient remains greater than 0.25. When $A = 1$, the promoting effect of the external force on diffusion completely disappears, causing $D_P(A)$ to return to 0.25.

An example illustrating this is the $D(A)$ curve under the influence of a periodic sinusoidal external force when $a = 3$, as depicted in Fig. 11. Within the $0 \leqslant A \leqslant 1$ range, the diffusion coefficients are all less than $D(A = 0) = 1/3$ with $a = 3$. This is because the system (5) without external force is in the series γ at $a = 3$, corresponding to a local maximum, so the external force disrupts this efficient particle diffusion.

Let's revisit the topic of $D(A)$. As shown in Fig. 10, the $D_P(A)$ curve exhibits a local maximum at $A = 0.5$ (also the maximum value with $0 \leqslant A \leqslant 1$). We have previously

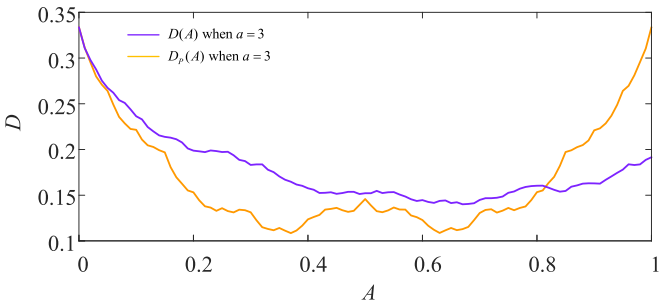

FIG. 11. The force-affected system's $D(A)$ and $D_P(A)$ curve at $a = 3$ differs from Fig. 10 because the external force inhibits the diffusion of particles, resulting in a reduction of its diffusion coefficient.

established that the particle escape efficiency is highest when subjected to a periodic pulse at $A = 0.5$. However, one observes that the peak of the $D(A)$ is not precisely situated at $A = 0.5$, but rather slightly shifted to the right. In addition to the previously mentioned explanation regarding the time-dependent external force sequence, another potential reason is that when A is slightly greater than 0.5, the presence of more values close to or equal to 0.5 in the sequence $F_S(A)$ continues to cause the diffusion coefficient $D(A)$ to increase, until the influence of the external force elements in the sequence $F_S(A)$ that have a negative effect on particle escape becomes predominant. Here, a critical value is $A \approx 0.525$, within one period, the sequence $F_S(A)$ contains two pairs of elements 0.5 and -0.5, which also corresponds to its true peak in Fig. 10.

Based on the analysis, summary, and certain physical intuition, we propose an empirical formula for $D(A)$ as

$$D(A) = \langle D_P(A) \rangle_{A \in F_S'(A)}, \tag{21}$$

where $F_S'(A) = \{A \sin(0.1\pi t) | t = 0, 1, 2, \cdots, 9\}$, and $\langle D_P(A) \rangle$ represents its average value.

To validate the effectiveness of Eq. (21), we present the $D(A)$ curve obtained from Eq. (21) based on the purple curve $D_P(A)$ in Fig. 10, as illustrated in the subsequent figure.

In Fig. 12, the green curve $D(A)$ calculated by Eq. (21) retains the essential characteristics of the diffusion coefficient directly calculated by system (19) (purple curve). However,

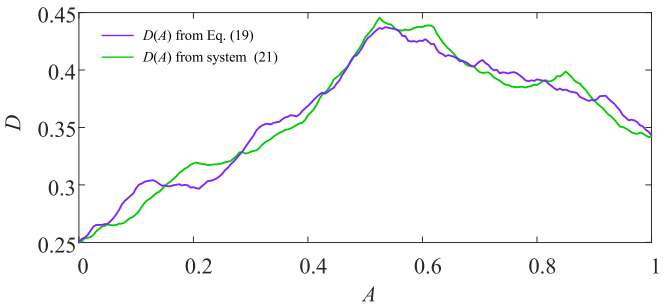

FIG. 12. The diffusion coefficient D, obtained from the EAMSD of a large number of particles using Eq. (19) (purple curve), demonstrates a comparable overall trend to the diffusion coefficient (green curve) obtained directly through Eq. (21). However, it exhibits distinct fluctuation patterns in finer structures.

there are some fluctuations that are not entirely consistent in more detailed aspects. Therefore, we believe that while the macroscopic phenomena of system (19) can be decomposed to some extent into simpler systems for characterization, the dynamic results exhibited by the collective behavior of the microscopic components at the underlying system level often manifest unexpected collective spatiotemporal patterns in complex systems. This may be an unexpected emergent phenomenon of complexity [88].

At a more detailed level of structure, the classification of turnstile dynamics based on "favorable" or "unfavorable" conditions appears in a more complex and irregular form, making it extremely difficult to predict the variation trend of $D(A)$, leading to fluctuation changes on an infinitely fine scale. Moreover, when A is large, especially for the region of $A \geqslant 3$, the curve is highly nontrivial, indicating limitations in interpreting the $D(A)$ curve using turnstile dynamics. In fact, the understanding of this unique structure of the $D(A)$ curve is still not fully sufficient.

Considering that Eq. (19) is a time-dependent nonautonomous dynamical system, and its motion range occurs over the entire real number domain for $t \to \infty$, for the convenience of analysis, we consider the motion to occur in a symmetric interval $L = [-l, l]$. We impose periodic boundary conditions, and the system can be considered as a nonhomogeneous Markov chain. Obviously, the calculation of its t-step transition matrix should be

$$P^{(t)} = \prod_{i=0}^{t} P^i P^{i-1} \cdots P^0, \tag{22}$$

where for each element within P^i, it should satisfy

$$\begin{cases} p_{i,i} = 0.5 - F_S/4, \\ p_{i,i+1} = 0.25 - F_S/4, \\ p_{i,i-1} = 0.25 + F_S/4, \\ p_{i,i-2} = F_S/4, \end{cases} \quad \text{when} \quad F_S > 0, \tag{23}$$

$$\begin{cases} p_{i,i} = 0.5 - F_S/4, \\ p_{i,i-1} = 0.25 - F_S/4, \\ p_{i,i+1} = 0.25 + F_S/4, \\ p_{i,i+2} = F_S/4, \end{cases} \quad \text{when} \quad F_S < 0. \tag{24}$$

When dealing with a probability transition matrix with absorbing boundary conditions, it takes the form of a block cyclic matrix, where each row is periodically shifted to the right. In Eq. (23), the boundary conditions $p_{1,2l+1} = 0.25 + A \sin(\Omega i)/4$, $p_{1,2l} = A \sin(\Omega i)/4$, $p_{2,2l+1} = A \sin(\Omega i)/4$, and $p_{2l+1,1} = 0.5 - A \sin(\Omega i)/4$ need to be supplemented, while the supplementation for Eq. (24) is not repeated. Consequently, P becomes a function of time. To ensure calculation accuracy, a larger range should be considered for the interval L when dealing with calculations on a larger timescale. We present the PDF in Fig. 13.

Figure 13 illustrates the PDF of the force-affected system (19) under different conditions. Unlike Fig. 4(a), the PDF of the system continues to exhibit an asymptotic Gaussian distribution. This partly explains why the overall EAMSD in Fig. 6(b) conforms to normal diffusion [89]. However, it is

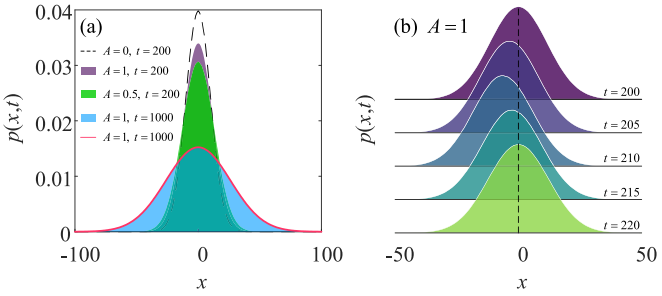

FIG. 13. (a) The frequency distribution plot of the system (19) and the red curve obtained from theoretical calculation [Eqs. (22)–(24)] show a Gaussian distribution fit. However, various external forces produce different PDFs, in line with the findings in Fig. 9. (b) The mean of the PDF varies periodically with iteration time, indicating the presence of aging phenomenon and EAMSD oscillation [see Figs. 6(b) and 14]. The PDFs are derived from trajectories of 10^7 uniformly distributed initial values x_0 on [0,1] and with L defined as $[-10000, 10000]$.

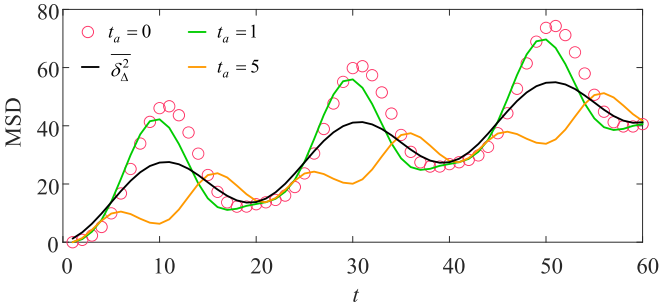

FIG. 14. The TAMSD of the force-affected system (19) and the EAMSD at different observation times t_a are both inconsistent with the EAMSD at $t_a = 0$ (red circle), indicating the presence of anomalous dynamics with ergodicity breaking and aging. The simulation parameters in Eq. (11) are set to $T = 3 \times 10^7$.

important to note that the PDF also displays some intriguing characteristics.

In Fig. 13(a), the purple and blue areas depict the PDF at external force amplitude $A = 1$ for iteration times $t = 200$ and 1000, both corresponding to a Gaussian distribution with a mean of zero. A longer iteration time results in a larger variance. However, when the external force amplitude is set to $A = 0.5$ and the iteration time to $t = 200$, the PDF curve is represented by the green area in the figure. It is evident that, in comparison to the purple area corresponding to $A = 1$, the green area exhibits a larger variance, indicating that particles may move a greater distance at the same time, implying $D(A = 0.5) > D(A = 1)$, indicating that the system has a larger diffusion coefficient, consistent with the conclusion in Fig. 10 and the analysis above. Moreover, the red curve represents the PDF obtained through Eqs. (22)–(24) with $A = 1$ and $t = 1000$, demonstrating the alignment between theory and simulation. Figure 13(b) demonstrates the periodic bias of the system's PDF. It is clear that the mean of the system's PDF has changed, suggesting aging behavior in the system, in line with the periodic oscillation of EAMSD in the system [Fig. 6(b)].

Using the same Eq. (11), the TAMSD of the system (19) is shown in the black curve in Fig. 14, indicating that the system also exhibits ergodicity breaking. Meanwhile, the green and orange curves in Fig. 14 represent the EAMSD of particles at different observation times, which are inconsistent with the EAMSD at observation time $t_a = 0$ represented by the red circle, indicating that the system also exhibits aging phenomena.

V. CONCLUSION

We hitherto concentrated on the anomalous behavior of a standard box piecewise linear map when subjected to various modes of external forces. Specifically, we examined the effects of two common types of external forces: linear and periodic. We focus on investigating key statistical parameters and their underlying generation mechanisms.

This paper initially delves into the impact of the linear external force, which is contingent on the particle's position, on the system's dynamics. The equal probability of particle escape in different directions is disrupted, prompting the particles to exhibit a greater tendency to move towards the cell facing the origin during each iteration. This, in turn, signifies the breakdown of the system's Gaussian PDF. We acknowledge that the diffusion of particles in this scenario is akin to a viscous Ehrenfest double urn model with reflecting walls. When subjected to a suitable external force, the particles move within a confined space, displaying a localized diffusion phenomenon consistent with the convergent EAMSD findings. Simultaneously, our characterization of the system's TAMSD and aging EAMSD illustrates its ergodicity breaking, aging anomalous dynamical behavior. In addition, its EAMSD in the long-term gradual process is somewhat equivalent to the Langevin equation in a harmonic potential.

For periodic external forces, they display delayed antipersistent random walks. A surprising finding is the presence of a "multipeak" fractal structure in the fitted diffusion coefficient, which correlates with the amplitude function of the external force. While we have conducted a certain degree of analysis on the dynamics of the turnstile, it must be acknowledged that a more fundamental explanation still requires further exploration. Furthermore, the PDF of a periodic external force asymptotically approaches a Gaussian distribution, indicating a partial fit with normal diffusion behavior. Furthermore, the system also demonstrates anomalous dynamical characteristics related to aging and ergodicity breaking.

Although deterministic chaotic systems are commonly used to elucidate real physical phenomena, it is necessary to consider the chaotic effects stemming from the vast and intricate networks of human society or nature. Thus, some chaotic systems may initially be employed to explain other intriguing phenomena, such as the well-known Logistic model [90]. When considering the external forces studied in this paper as more abstract, for instance, in the model (7), the population increase exacerbating carbon emissions, impacting climate change, and consequently affecting mortality, and subsequently influencing population growth [91]. The connection between demographic dynamics and chaotic diffusion is worth further consideration. Along these lines, in the context

of model (19), a periodic external force can be interpreted as cyclical financial crises in the international market. The cyclical recurrence of these long-wave crises is likely to either drive successive surges of innovative clusters leading to technological change, or instigate a new round of economic prosperity [92]. However, it is important to note that when a stable system without external forces is at its peak, these cyclical blows may also exert a significant inhibitory effect on it (Fig. 11). This association is highly intriguing and presents an open interesting proposition.

ACKNOWLEDGMENTS

This work is supported by the National Natural Science Foundation of China (Grants No. 62071496 and No. 62061008).

[1] V. Zaburdaev, S. Denisov, and J. Klafter, Lévy walks, Rev. Mod. Phys. **87**, 483 (2015).
[2] J. Szymański and M. Weiss, Elucidating the origin of anomalous diffusion in crowded fluids, Phys. Rev. Lett. **103**, 038102 (2009).
[3] A. V. Weigel, B. Simon, M. M. Tamkun, and D. Krapf, Ergodic and nonergodic processes coexist in the plasma membrane as observed by single-molecule tracking, Proc. Natl. Acad. Sci. USA **108**, 6438 (2011).
[4] G. Seisenberger, M. U. Ried, T. Endress, H. Büning, M. Hallek, and C. Bräuchle, Real-time single-molecule imaging of the infection pathway of an adeno-associated virus, Science **294**, 1929 (2001).
[5] G. Boffetta and I. M. Sokolov, Relative dispersion in fully developed turbulence: The Richardson's law and intermittency corrections, Phys. Rev. Lett. **88**, 094501 (2002).
[6] E. W. Montroll and G. H. Weiss, Random walks on lattices, J. Math. Phys. **6**, 167 (1965).
[7] R. Metzler, J.-H. Jeon, A. G. Cherstvy, and E. Barkai, Anomalous diffusion models and their properties: Nonstationarity, non-ergodicity, and ageing at the centenary of single particle tracking, Phys. Chem. Chem. Phys. **16**, 24128 (2014).
[8] J. Nelson, Continuous-time random-walk model of electron transport in nanocrystalline TiO_2 electrodes, Phys. Rev. B **59**, 15374 (1999).
[9] Y. Meroz and I. M. Sokolov, A toolbox for determining subdiffusive mechanisms, Phys. Rep. **573**, 1 (2015).
[10] J. M. Sancho, A. M. Lacasta, K. Lindenberg, I. M. Sokolov, and A. H. Romero, Diffusion on a solid surface: Anomalous is normal, Phys. Rev. Lett. **92**, 250601 (2004).
[11] V. Zaburdaev, S. Denisov, and P. Hänggi, Space-time velocity correlation function for random walks, Phys. Rev. Lett. **110**, 170604 (2013).
[12] A. Rebenshtok, S. Denisov, P. Hänggi, and E. Barkai, Nonnormalizable densities in strong anomalous diffusion: Beyond the central limit theorem, Phys. Rev. Lett. **112**, 110601 (2014).
[13] M. Yang and M. Ripoll, Brownian motion in inhomogeneous suspensions, Phys. Rev. E **87**, 062110 (2013).
[14] E. Racca and A. Porporato, Langevin equations from time series, Phys. Rev. E **71**, 027101 (2005).
[15] A. Malsagov and M. Mandjes, Approximations for reflected fractional Brownian motion, Phys. Rev. E **100**, 032120 (2019).
[16] A. Maćkała and M. Magdziarz, Statistical analysis of superstatistical fractional Brownian motion and applications, Phys. Rev. E **99**, 012143 (2019).
[17] H. Scher and E. W. Montroll, Anomalous transit-time dispersion in amorphous solids, Phys. Rev. B **12**, 2455 (1975).
[18] T. H. Solomon, E. R. Weeks, and H. L. Swinney, Observation of anomalous diffusion and Lévy flights in a two-dimensional rotating flow, Phys. Rev. Lett. **71**, 3975 (1993).
[19] Fogedby, Langevin equations for continuous time Lévy flights, Phys. Rev. E **50**, 1657 (1994).
[20] D. Schertzer, M. Larchev, J. Duan, V. V. Yanovsky, and S. Lovejoy, Fractional Fokker-Planck equation for nonlinear stochastic differential equations driven by non-Gaussian Levy stable noises, J. Math. Phys. **42**, 200 (2001).
[21] M. S. Alrawashdeh, J. F. Kelly, M. M. Meerschaert, and H.-P. Scheffler, Applications of inverse tempered stable subordinators, Comput. Math. Appl. **73**, 892 (2017).
[22] A. Cairoli and A. Baule, Langevin formulation of a subdiffusive continuous-time random walk in physical time, Phys. Rev. E **92**, 012102 (2015).
[23] D. G. Díaz, Inverse relationship between diffusion coefficient and mass for a free particle system: Approach by using maximum caliber principle and monte carlo simulations, Chaos **32**, 123141 (2022).
[24] Stepanow, Velocity drift of a Brownian particle in a random environment, Phys. Rev. A **43**, 2771 (1991).
[25] K. Lindenberg, A. M. Lacasta, J. M. Sancho, and A. H. Romero, Transport and diffusion on crystalline surfaces under external forces, New J. Phys. **7**, 29 (2005).
[26] G. A. Pavliotis, A multiscale approach to Brownian motors, Phys. Lett. A **344**, 331 (2005).
[27] S. Eule, R. Friedrich, F. Jenko, and D. Kleinhans, Langevin approach to fractional diffusion equations including inertial effects, J. Phys. Chem. B **111**, 11474 (2007).
[28] A. Weron, M. Magdziarz, and K. Weron, Modeling of subdiffusion in space-time-dependent force fields beyond the fractional Fokker-Planck equation, Phys. Rev. E **77**, 036704 (2008).
[29] M. Magdziarz, A. Weron, and J. Klafter, Equivalence of the fractional Fokker-Planck and subordinated Langevin equations: The case of a time-dependent force, Phys. Rev. Lett. **101**, 210601 (2008).
[30] S. Burov, R. Metzler, and E. Barkai, Aging and nonergodicity beyond the Khinchin theorem, Proc. Natl. Acad. Sci. USA **107**, 13228 (2010).
[31] P. Dieterich, R. Klages, and A. V. Chechkin, Fluctuation relations for anomalous dynamics generated by time-fractional Fokker–Planck equations, New J. Phys. **17**, 075004 (2015).
[32] S. P. Fedotov and N. Korabel, Subdiffusion in an external potential: Anomalous effects hiding behind normal behavior, Phys. Rev. E **91**, 042112 (2015).

[33] A. Cairoli and A. Baule, Erratum: Anomalous processes with general waiting times: Functionals and multipoint structure, Phys. Rev. Lett. **120**, 259902(E) (2018).
[34] Y. Chen, X. Wang, and W. Deng, Tempered fractional Langevin–Brownian motion with inverse β-stable subordinator, J. Phys. A: Math. Theor. **51**, 495001 (2018).
[35] Y. Chen, X. Wang, and W. Deng, Subdiffusion in an external force field, Phys. Rev. E **99**, 042125 (2019).
[36] X. Wang and Y. Chen, Random diffusivity processes in an external force field, Phys. Rev. E **106**, 024112 (2022).
[37] X. Wang and Y. Chen, Langevin picture of anomalous diffusion processes in expanding medium, Phys. Rev. E **107**, 024105 (2023).
[38] G. J. Morales, Two-dimensional chaotic thermostat and behavior of a thermalized charge in a weak magnetic field, Phys. Rev. E **99**, 062218 (2019).
[39] A. S. Pikovsky, Transition to synchrony in chiral active particles, J. Phys.: Complex. **2**, 025009 (2021).
[40] M. F. Shlesinger, G. Zaslavsky, and J. Klafter, Strange kinetics, Nature (London) **363**, 31 (1993).
[41] J. Klafter, M. F. Shlesinger, and G. Zumofen, Beyond Brownian motion, Phys. Today **49**(2), 33 (1996).
[42] A. Zacherl, T. Geisel, J. Nierwetberg, and G. Radons, Power spectra for anomalous diffusion in the extended Sinai billiard, Phys. Lett. A **114**, 317 (1986).
[43] G. Zaslavsky, Chaos, fractional kinetics, and anomalous transport, Phys. Rep. **371**, 461 (2002).
[44] T. Geisel and S. Thomae, Anomalous diffusion in intermittent chaotic systems, Phys. Rev. Lett. **52**, 1936 (1984).
[45] G. Zumofen and J. Klafter, Scale-invariant motion in intermittent chaotic systems, Phys. Rev. E **47**, 851 (1993).
[46] N. Korabel, A. V. Chechkin, R. Klages, I. M. Sokolov, and V. Yu. Gonchar, Understanding anomalous transport in intermittent maps: From continuous-time random walks to fractals, Europhys. Lett. **70**, 63 (2005).
[47] N. Korabel, R. Klages, A. V. Chechkin, I. M. Sokolov, and V. Y. Gonchar, Fractal properties of anomalous diffusion in intermittent maps, Phys. Rev. E **75**, 036213 (2007).
[48] E. Barkai, Aging in subdiffusion generated by a deterministic dynamical system, Phys. Rev. Lett. **90**, 104101 (2003).
[49] B. A. Huberman, J. P. Crutchfield, and N. H. Packard, Noise phenomena in Josephson junctions, Appl. Phys. Lett. **37**, 750 (1980).
[50] D. D'Humières, M. R. Beasley, B. A. Huberman, and A. Libchaber, Chaotic states and routes to chaos in the forced pendulum, Phys. Rev. A **26**, 3483 (1982).
[51] T. Geisel and J. Nierwetberg, Onset of diffusion and universal scaling in chaotic systems, Phys. Rev. Lett. **48**, 7 (1982).
[52] M. Schell, S. Fraser, and R. Kapral, Diffusive dynamics in systems with translational symmetry: A one-dimensional-map model, Phys. Rev. A **26**, 504 (1982).
[53] H. Fujisaka and S. K. Grossmann, Chaos-induced diffusion in nonlinear discrete dynamics, Z. Phys. B: Condens. Matter **48**, 261 (1982).
[54] R. Klages and J. R. Dorfman, Simple maps with fractal diffusion coefficients, Phys. Rev. Lett. **74**, 387 (1995).
[55] R. Klages and J. R. Dorfman, Simple deterministic dynamical systems with fractal diffusion coefficients, Phys. Rev. E **59**, 5361 (1999).
[56] Y. Sato and R. Klages, Anomalous diffusion in random dynamical systems, Phys. Rev. Lett. **122**, 174101 (2019).
[57] R. Kazakevičius and J. Ruseckas, Influence of external potentials on heterogeneous diffusion processes, Phys. Rev. E **94**, 032109 (2016).
[58] D. Berman, S. A. Deshmukh, S. K. Sankaranarayanan, A. Erdemir, and A. V. Sumant, Macroscale superlubricity enabled by graphene nanoscroll formation, Science **348**, 1118 (2015).
[59] T. Papamarkou and A. J. Lawrance, Nonlinear dynamics of trajectories generated by fully-stretching piecewise linear maps, Int. J. Bifurcat. Chaos **24**, 1450071 (2014).
[60] J. L. Palacios, Fluctuation theory for the Ehrenfest urn via electric networks, Adv. Appl. Probab. **25**, 472 (1993).
[61] C.-H. Cheng, B. Gemao, and P.-Y. Lai, Phase transitions in Ehrenfest urn model with interactions: Coexistence of uniform and nonuniform states, Phys. Rev. E **101**, 012123 (2020).
[62] A. Kolmogoroff, Über die analytischen methoden in der wahrscheinlichkeitsrechnung, Math. Ann. **104**, 415 (1931).
[63] A. M. Kamińska and T. Srokowski, Solving the Chapman-Kolmogorov equation for a jumping process, Phys. Rev. E **67**, 061114 (2003).
[64] J. Hierro and C. Dopazo, Singular boundaries in the forward Chapman-Kolmogorov differential equation, J. Stat. Phys. **137**, 305 (2009).
[65] I. Nordlund, Eine neue bestimmung der avogadroschen konstante aus der brownschen bewegung kleiner, in wasser suspendierten quecksilberkügelchen, Z. Phys. Chem. **87U**, 40 (1914).
[66] Y. He, S. Burov, R. Metzler, and E. Barkai, Random time-scale invariant diffusion and transport coefficients, Phys. Rev. Lett. **101**, 058101 (2008).
[67] A. Lubelski, I. M. Sokolov, and J. Klafter, Nonergodicity mimics inhomogeneity in single particle tracking, Phys. Rev. Lett. **100**, 250602 (2008).
[68] J.-H. Jeon and R. Metzler, Inequivalence of time and ensemble averages in ergodic systems: Exponential versus power-law relaxation in confinement, Phys. Rev. E **85**, 021147 (2012).
[69] J.-H. Jeon, N. Leijnse, L. B. Oddershede, and R. Metzler, Anomalous diffusion and power-law relaxation of the time averaged mean-squared displacement in worm-like micellar solutions, New J. Phys. **15**, 045011 (2013).
[70] L. Laloux and P. Le Doussal, Aging and diffusion in low dimensional environments, Phys. Rev. E **57**, 6296 (1998).
[71] S. Burov and E. Barkai, Occupation time statistics in the quenched trap model, Phys. Rev. Lett. **98**, 250601 (2007).
[72] R. Metzler and J. Klafter, The random walk's guide to anomalous diffusion: A fractional dynamics approach, Phys. Rep. **339**, 1 (2000).
[73] J. Paneva-Konovska, Overconvergence of series in generalized Mittag-Leffler functions, Fract. Calc. Appl. Anal. **20**, 506 (2017).
[74] A. L. Demirel and S. Granick, Friction fluctuations and friction memory in stick-slip motion, Phys. Rev. Lett. **77**, 4330 (1996).
[75] M. Gitterman, Harmonic oscillator with fluctuating damping parameter, Phys. Rev. E **69**, 041101 (2004).
[76] A. V. Dyskin and E. Pasternak, Bifurcation in rolling of non-spherical grains and fluctuations in macroscopic friction, Acta Mech. **225**, 2217 (2014).
[77] M. Urbakh, J. Klafter, D. Gourdon, and J. N. Israelachvili, The nonlinear nature of friction, Nature (London) **430**, 525 (2004).

[78] A. Vanossi, N. Manini, M. Urbakh, S. Zapperi, and E. Tosatti, Colloquium: Modeling friction: From nanoscale to mesoscale, Rev. Mod. Phys. **85**, 529 (2013).

[79] Q. Li, Y. Dong, D. Perez, A. Martini, and R. W. Carpick, Speed dependence of atomic stick-slip friction in optimally matched experiments and molecular dynamics simulations, Phys. Rev. Lett. **106**, 126101 (2011).

[80] I. Barel, M. Urbakh, L. Jansen, and A. Schirmeisen, Unexpected temperature and velocity dependencies of atomic-scale stick-slip friction, Phys. Rev. B **84**, 115417 (2011).

[81] E. Riedo, E. Gnecco, R. Bennewitz, E. Meyer, and H. Brune, Interaction potential and hopping dynamics governing sliding friction, Phys. Rev. Lett. **91**, 084502 (2003).

[82] E. Riedo and H. Brune, Young modulus dependence of nanoscopic friction coefficient in hard coatings, Appl. Phys. Lett. **83**, 1986 (2003).

[83] J. Servantie and P. Gaspard, Methods of calculation of a friction coefficient: Application to nanotubes, Phys. Rev. Lett. **91**, 185503 (2003).

[84] G.-P. Ostermeyer, On the dynamics of the friction coefficient, Wear **254**, 852 (2003).

[85] K. Tian, D. L. Goldsby, and R. W. Carpick, Rate and state friction relation for nanoscale contacts: Thermally activated Prandtl-Tomlinson model with chemical aging, Phys. Rev. Lett. **120**, 186101 (2018).

[86] P. Tierno, F. Sagués, T. H. Johansen, and I. M. Sokolov, Antipersistent random walk in a two state flashing magnetic potential, Phys. Rev. Lett. **109**, 070601 (2012).

[87] T. Albers, D. Müller-Bender, and G. Radons, Antipersistent random walks in time-delayed systems, Phys. Rev. E **105**, 064212 (2022).

[88] Z. Zheng, Q. Ma, Z. Bi, S. C. de la Barrera, M.-H. Liu, N. Mao, Y. Zhang, N. Kiper, K. Watanabe, T. Taniguchi, J. Kong, W. A. Tisdale, R. C. Ashoori, N. Gedik, L. Fu, S.-Y. Xu, and P. Jarillo-Herrero, Unconventional ferroelectricity in moiré heterostructures, Nature (London) **588**, 71 (2020).

[89] Y. Han, A. M. Alsayed, M. Nobili, J. Zhang, T. C. Lubensky, and A. G. Yodh, Brownian motion of an ellipsoid, Science **314**, 626 (2006).

[90] R. M. May, Simple mathematical models with very complicated dynamics, Nature (London) **261**, 459 (1976).

[91] V. Lupi and S. Marsiglio, Population growth and climate change: A dynamic integrated climate-economy-demography model, Ecol. Econ. **184**, 107011 (2021).

[92] B. J. L. Berry, A pacemaker for the long wave, Technol. Forecast. Soc. Change **63**, 1 (2000).